Supplementary Information

Age, lipofuscin and melanin oxidation affect fundus near-infrared autofluorescence

Tatjana Taubitz, Yuan Fang, Antje Biesemeier, Sylvie Julien-Schraermeyer, Ulrich Schraermeyer

Tatjana Taubitz
Email: tatjana.taubitz@med.uni-tuebingen.de

This supplementary information includes:

Figs. S1 to S8

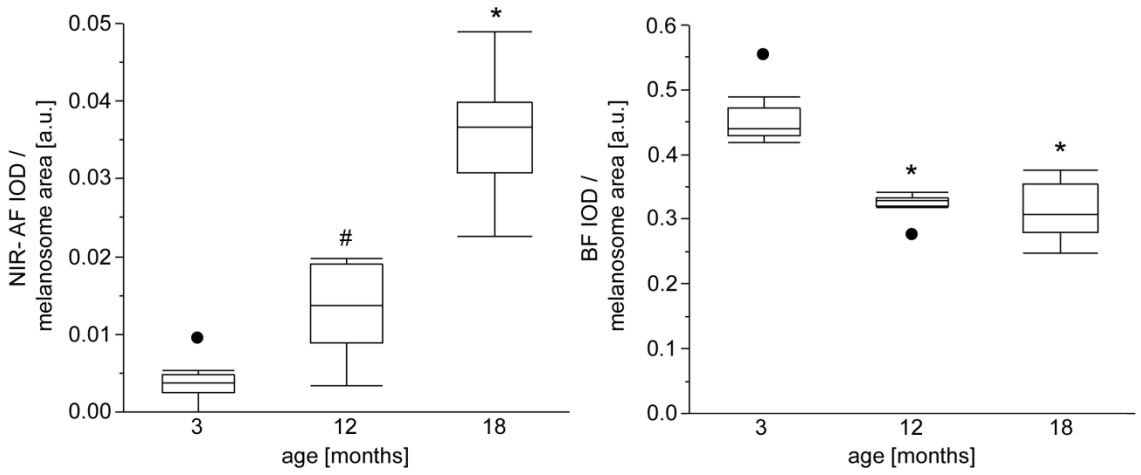

Figure S1. Semi-quantitative analysis of total NIR-AF (left) and BF (right) intensities derived from RPE and choroid of WT mice (N = 7-11 pictures per group, # $p < 0{\cdot}01$, * $p < 0{\cdot}0001$, Dunnett's test). AF: autofluorescence; BF: bright field; IOD: integrated optical density; NIR: near-infrared.

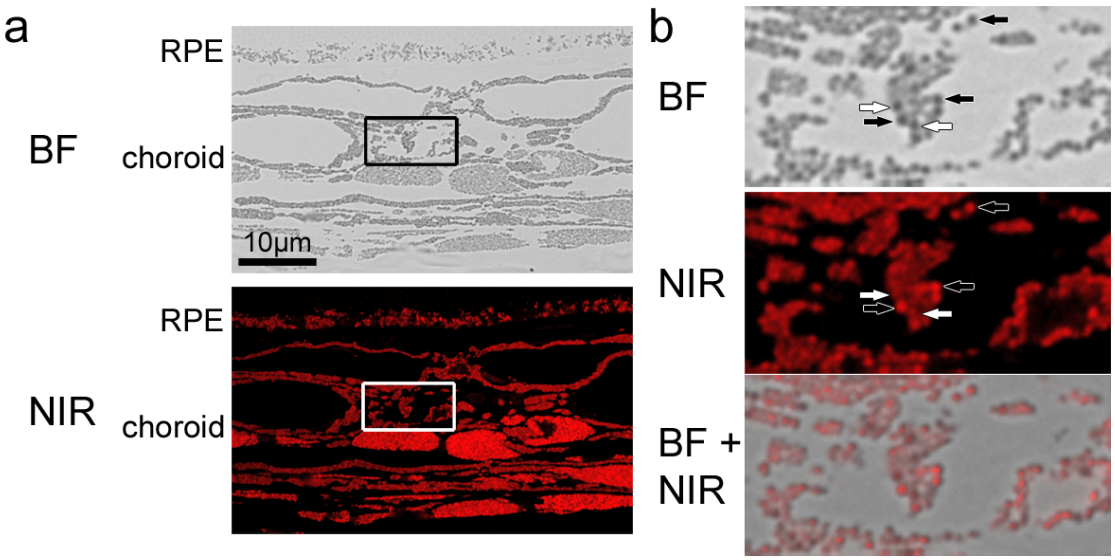

Figure S2. Choroidal melanosomes differ in their NIR-AF properties. Bright field and post-processed NIR-AF micrographs of an 18-month-old WT mouse. Boxed areas in a) are shown magnified in b). Even though melanosomes have similar size and density in bright field, they can show either very intense (black arrows) or very weak (white arrows) NIR-AF. Also note the large, roundish cells with high levels of NIR-AF in the choroid that are macrophage-like cells (compare with Fig. 2). BF: bright field; NIR: near-infrared.

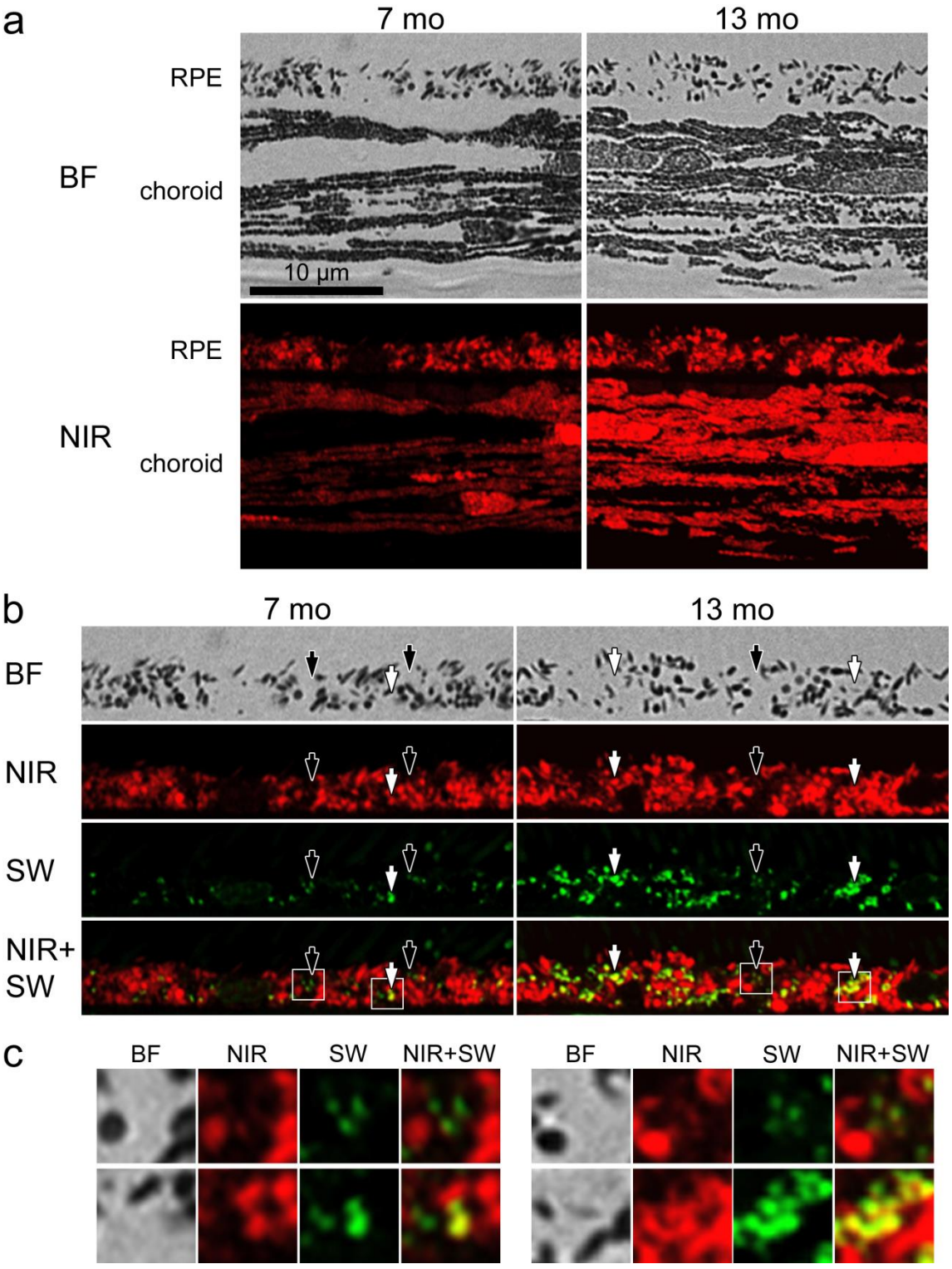

Figure S3. Comparison of 7- and 13-month-old pigmented *Abca4*$^{-/-}$ mice. a) Overview of RPE and choroidal NIR-AF (red) taken under identical conditions. Note the large, roundish cells with high levels of NIR-AF in the choroid of the 13-month-old animal that are macrophage-like cells (compare with Fig. 2). b) Magnified BF and NIR-AF (red) and SW-AF (green) images of the RPE areas shown in (a). AF images were post-processed to allow the localization of weak signals. White arrows point to lipofuscin with prominent NIR-AF signal, resulting in yellow colour in overlay images, while black arrows point to lipofuscin with no or limited NIR-AF signal, resulting in green colour in overlay images. Boxed areas are magnified in (c). c) Magnified images of the boxed areas in (b). Top row shows black arrow areas, bottom row shows white arrow areas. BF: bright field; NIR: near-infrared; SW: short wavelength.

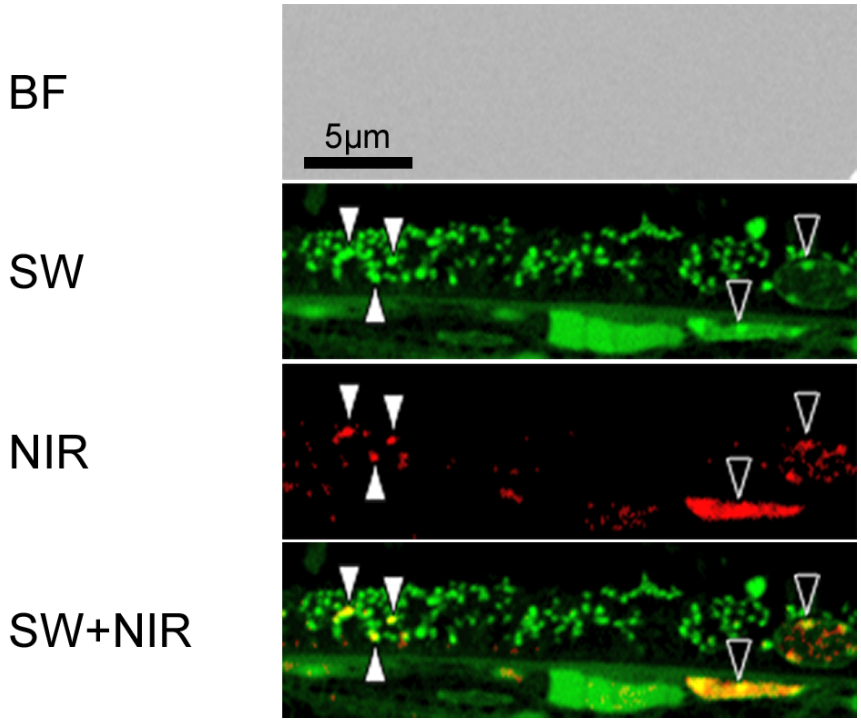

Figure S4. Autofluorescence in the RPE of a 12-month-old albino *Abca4*$^{-/-}$ mouse. The bright field image shows no tissue structures due to lack of melanin in albino animals and no additional staining. AF images were post-processed to allow the localization of weak signals. Areas exhibiting both AF modalities are yellow in the superimposed image. Few lipofuscin granules show NIR-AF signals (white arrowheads) that are not stronger than background signals derived from RPE and choroidal nuclei (black arrowheads). BF: bright field; NIR: near-infrared; SW: short wavelength.

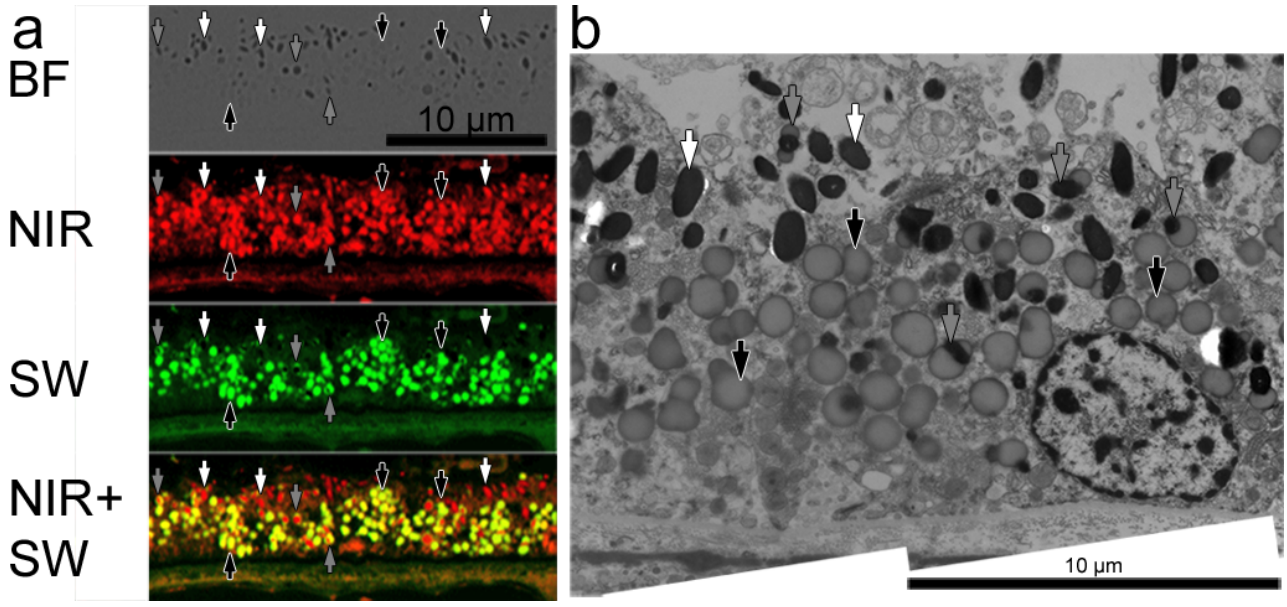

Figure S5. Autofluorescence and electron microscopy of the RPE of a 80-year-old human donor. a) NIR-AF (red) and SW-AF (green) images were post-processed to allow the localization of weak signals. Yellow colour shows areas where NIR-AF and SW-AF superimpose. In aged human RPE, melanosomes (white arrows) are reduced and mostly found apically. Many BF-identified melanosomes are surrounded by SW-AF identified lipofuscin, indicative of melanolipofuscin (grey arrows). Lipofuscin granules are marked with black arrows and predominantly show both NIR- and SW-AF. b) Routine ultrastructural image (post-fixed with osmium tetroxide, stained with uranyl acetate and lead citrate) from the same eye, pigment granules are labelled identical as in a). BF: bright field; NIR: near-infrared; SW: short wavelength.

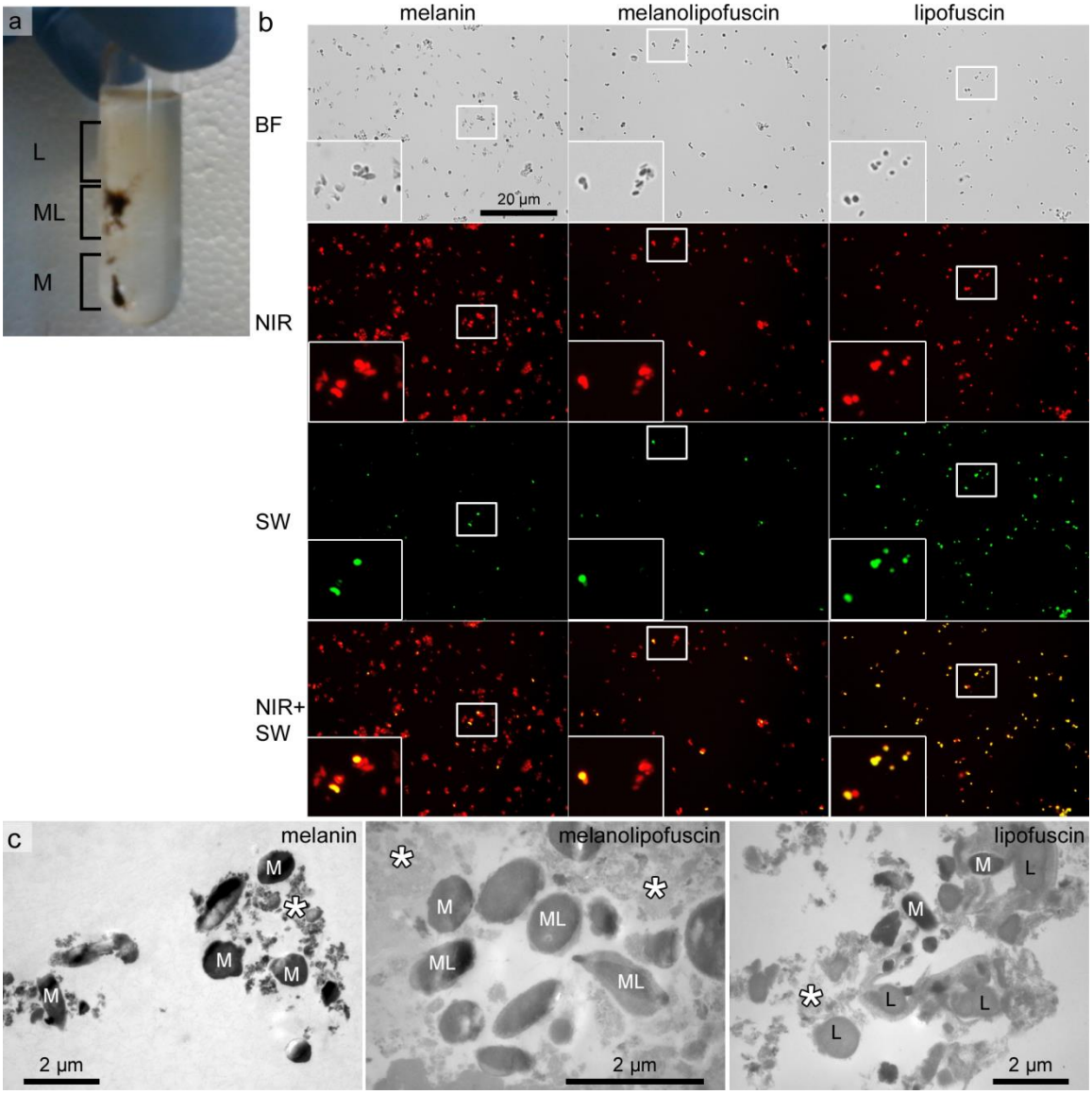

Figure S6. NIR-AF and SW-AF of isolated human RPE granules (46 – 91 years old, mean age 70·2 ± 14·7 years). a) RPE granules were separated by density gradient centrifugation into three fractions containing lipofuscin (L), melanolipofuscin (ML) and melanin (M), respectively. b) NIR-AF (red) and SW-AF (green) images of isolated granules were post-processed to allow the localization of weak signals. Yellow colour in NIR-/SW-AF overlay images shows areas where NIR-AF and SW-AF superimpose. Insets show magnifications of the boxed areas. c) Electron micrographs of granules from the three isolated fractions. Note that granules are surrounded by extragranular debris (asterisks), as has been described before[1]. BF: bright field; NIR: near-infrared; SW: short wavelength.

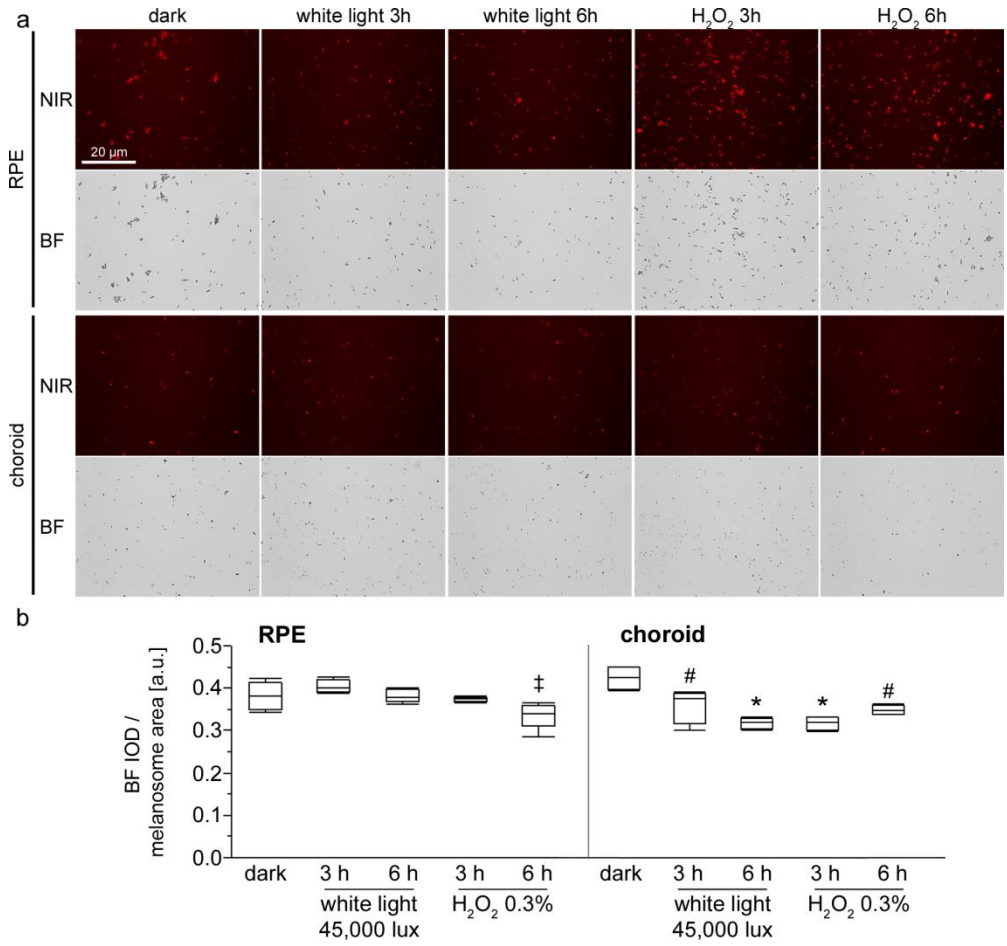

Figure S7. Porcine RPE and choroidal melanosomes after photic and oxidative stress. Isolated melanosomes were either kept in the dark (control) or treated with white light (45,000 lux) or with 0·3% hydrogen peroxide at pH 7·4 for 3 to 6 hours, respectively. a) Representative NIR-AF and BF images of the different groups. b) Semi-quantitative analysis of melanosome darkness in bright field images. Choroidal melanosomes react more readily with granule brightening than RPE melanosomes, while RPE melanosomes predominately react to photic and oxidative stress with presence of NIR-AF (see Fig. 7 in main text). (N = 4-6 images per group, ‡ $p < 0{\cdot}05$, # $p < 0{\cdot}01$, * $p < 0{\cdot}0001$, Dunnett's test). BF: bright field; IOD: integrated optical density; NIR: near-infrared.

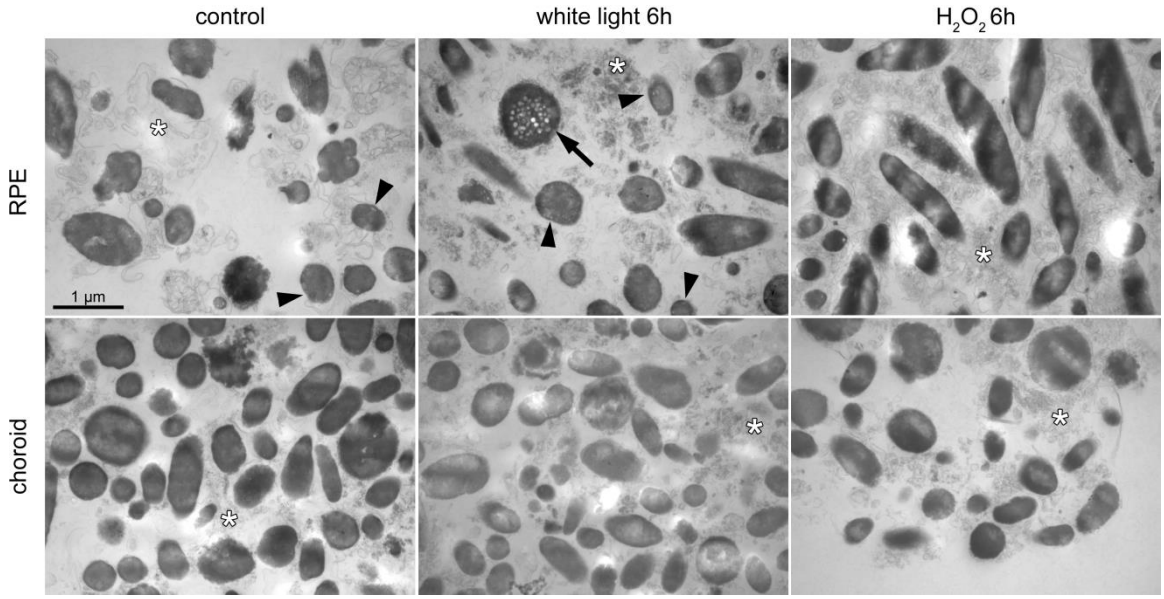

Figure S8. Ultrastructural changes of porcine RPE and choroidal melanosomes after photic and oxidative stress. Control RPE melanosomes have a relatively homogenous electron dense presence and occasionally show small holes close to the granule edge (arrowheads). After treatment with white light, these holes appear more often in RPE melanosomes and seem to increase in size. Individual melanosomes present with numerous big holes throughout the granule profile (arrow). In hydrogen peroxide treated RPE melanosomes, the holes are less prominent, but the formerly relative homogenous electron density appears striated. In choroidal melanosomes, ultrastructural changes are much less prominent. Note that granules are surrounded by extragranular debris (asterisks), as has been described before[1].

References

1. Ng KP, Gugiu B, Renganathan K, et al. Retinal pigment epithelium lipofuscin proteomics. *Molecular & cellular proteomics : MCP* 2008; **7**: 1397–405.